Enhanced Measurement Technique for Lens Centering Error with Power Analysis and Subwavelength Grating-Patterned Prism Module

Yu-Zhen Mao,[1] Chin-Ting Ho,[1] Shiau-Cheng Shiu,[1] and Chun-Wei Liu,[1,#]

1 National Tsing Hua University, Power Mechanical Engineering, Section 2, Guangfu Road, Hsinchu, 300044, Taiwan
Corresponding Author / Email: weilu@pme.nthu.edu.tw, TEL: +886-03-5742914

KEYWORDS:Lens centering error, Subwavelength grating, Power meter

This study presents a technique for accurately measuring the centering error of a lens. The proposed technique integrates power analysis, employing a prism module patterned with a subwavelength grating, in conjunction with a reflection-centering system utilizing the −1st-order rays at 5 mW and 650 nm. By leveraging Snell's law and diffractive characteristics, the centering error is thoroughly tested and analyzed using a power meter. Compared to the conventional autocollimation-based centering error measuring system, the proposed technique demonstrates a fourfold amplification in the resolution of optical centering error within the system. The introduced technique in this study enhances instrument sensitivity by exploiting variations in the direction and energy of light.

NOMENCLATURE

θ_{diff} = the angle of diffraction
θ_{inc} = the incidence angle of diffraction surface
m = the diffraction order
λ = the wavelength of the incident ray
Λ = the grating period
n_{air} = the refractive index of air
n_p = the refractive index of prism
α = the incidence angle of prism
θ_p = the angle of prism
CP = the SWG surface topography
w = the peak position of SWG

1. Introduction

Measurement and control of centering error (CE) in optical component fabrication is crucial for high-quality imaging, optical instruments, and semiconductor manufacturing. Lenses with a low CE have better overall accuracy. The optical axis usually does not coincide with the mechanical axis after optical polishing of the surface during the optical fabrication process. resulting in decenter and tilt. Correcting CE through centering and edging reduces comet aberration, astigmatism, and field curvature.

Autocollimation is a widely used method to measure CE [1]. It computes CE from displacement measurements using an autocollimated image. Precise centering is essential to avoid damaging lens surfaces during cementing. Development of autocollimation instruments has improved efficiency and accuracy [2-3].

Two methods are used to measure laser spot variation at the receiving end for CE measurement. One involves etching more lines on the dividing plate for higher resolution, and the other improves the sensor resolution. To avoid chromatic aberration, single-wavelength light is typically used for measurement. To enhance accuracy, this study incorporates a subwavelength grating (SWG) into the optical setup, which diffracts light into different beams based on incident angles and spacing. SWGs are widely used in displays, refractive index measurement, and communication equipment [4-6]. They are now manufactured efficiently through roll-to-roll and laser processes, expanding their applications [7-10].

2. Subwavelength Grating-Patterned Prism Module

2.1 Optical Setup

This paper presents a novel technique for measuring lens centering error (CE) using roll-to-roll subwavelength grating (SWG) and power analysis. The method employs rigorous coupled-wave analysis diffraction efficiency of SWG and Snell's law. Compared to autocollimation-based systems, this technique achieves four times higher resolution for CE measurement. Experimental results with a

375-nm SWG and 5 mW 650-nm laser show subarcsecond accuracy. The setup in Fig. 1 involves a collimated laser passing through a beam splitter and objective lens to reach the test lens. The reflected beam passes through SWG surfaces on a prism and is measured by a power meter, with changes in power indicating CE variations.

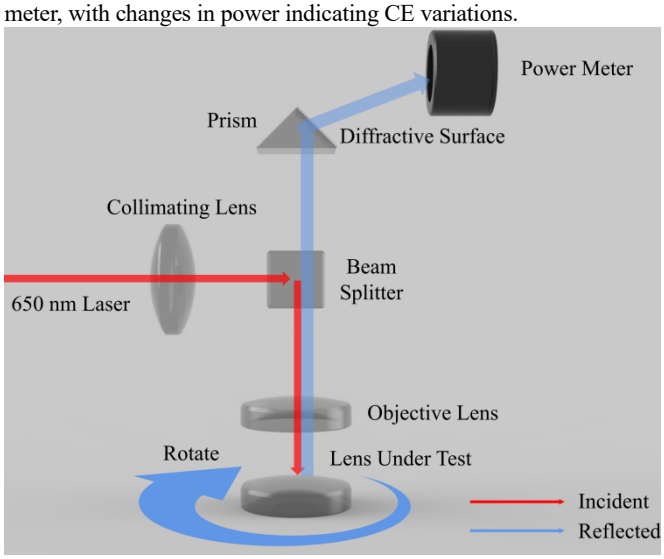

Fig. 1 Optical pathway of the measurement system

In this study, the measurement technique utilized a diffraction light of -1st order, as it offers superior amplification of angle variation while reducing the power of the diffracted beam. To optimize the sensitivity of the diffraction angle and diffraction efficiency, the parameters of the prism and the surface of the SWG were carefully optimized. The SWG was manufactured using ultraprecision machining with a single-point diamond tool [11-12]. The design of the SWG profiles and the prism angle were taken into consideration. Fig. 2 illustrates the optical path within the prism pattern through the SWG.

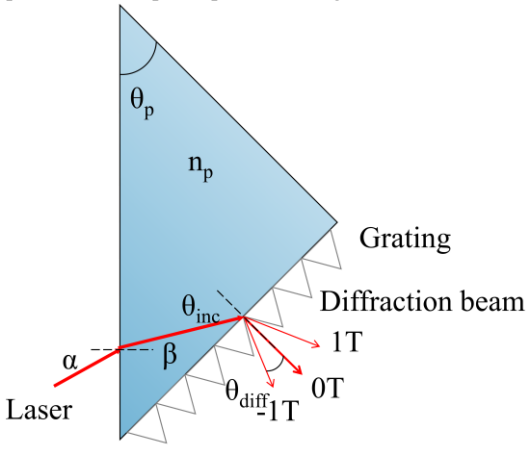

Fig. 2 Optical pathway in the prism using SWG

The relationship between the angle of diffraction θ_{diff} and the angle of incidence θ_{inc} on the SWG is determined through application of the grating equation [13], which is expressed as follows:

$$\theta_{diff} = \frac{\sin^{-1}\left(m\frac{\lambda}{\Lambda}+n_p\sin\left(\sin^{-1}\left(\frac{n_{air}\sin\alpha}{n_p}\right)+\theta_p\right)\right)}{n_{air}}, \quad (1)$$

where m is the diffraction order, λ is the wavelength of the incident ray, and Λ is the grating period, n_{air} is 1 and the refractive index n_p is 1.5. On this basis, the parameters m, λ, α, and θ_p must be further discussed.

2.2 Simulation

Fig. 3 depicts the plot of θ_{diff} against θ_{inc} with different λ/Λ based on Eq. (3). The zero-order diffraction beam only followed Snell's law, regardless of the changes to the grating period; the θ_{inc} remained at 41.8182° when the θ_{diff} was 90°. To avoid the interference of other-order diffraction light, θ_{inc} was set between 41.8182° and 52.7273°. When the beam exited from SWG, only −1st-order beam was present.

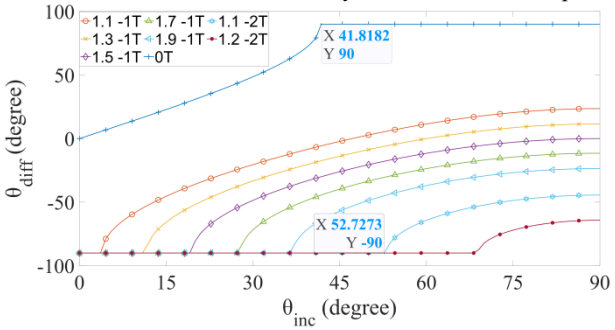

Fig. 3 Relationship between θ_{inc} and θ_{diff} with different ratios of wavelength and grating periods

Therefore, according to the results presented in Fig. 3, with a wavelength of 650 nm and a grating period from 350 to 550 nm, the influence of the incident angle and SWG morphology on diffraction efficiency was further examined.

To evaluate the effect of SWG surface topography on diffraction efficiency, a parameter called *CP*, representing the ratio of the peak position w to the period Λ, was analyzed (Fig. 4). $CP = 0.5$ was chosen based on previous research considering fabrication capabilities and diffraction efficiency [14], and it was applied in this study.

Table 1 provides the calculated values for λ/Λ, incident angles θ_{inc}, diffraction angles θ_{diff}, as well as the wavelengths, SWG morphology, and other relevant parameters. Using these data, the influence of diffraction efficiency was simulated, and the results are shown in Fig. 5.

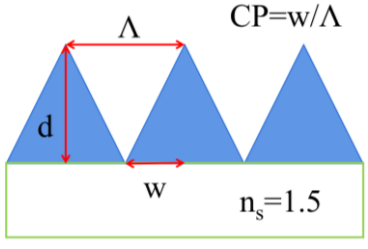

Fig. 4 Surface structure of the SWG

Table 1 SWG parameter setting

Laser Wavelength	650 nm
Grating Depth	0 - 1000nm
Grating Shape	triangle
Prism Refractive Index	1.5
Angle of Incident Light	40°,45°,50°
Grating period	350 - 550nm
CP	0.5

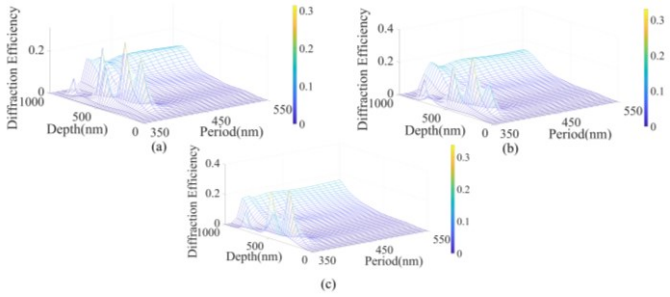

Fig. 5 Relationship between grating depth and average diffraction efficiency of (a) $\theta_{inc} = 40°$, (b) $\theta_{inc} = 45°$, and (c) $\theta_{inc} = 50°$ at $CP = 0.5$

The simulation results presented in Fig. 5 revealed that the maximum diffraction efficiency was achieved in the grating period range of 350 to 400 nm. For incident angles θ_{inc} of 45° and 50°, the grating depth d was approximately in the range of 300 to 500 nm. Considering the subsequent experiments and the universal applicability of the prism, the analysis was performed using the following settings: grating period $\Lambda = 375$ nm and incident angle $\theta_{inc} = 45°$.

With the SWG surface shape and incident angle determined, the magnification effects were examined. Equation 1 was used for the calculations, and Fig. 6 illustrates the effect of angular amplification at different prism angles θ_p)when the beam reaches the surface of the prism vertically ($\alpha = 0$).

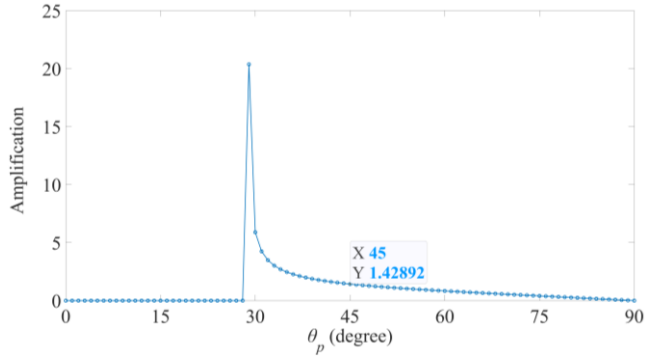

Fig. 6 Angle amplification effect of different θ_p

Under the prism angle of $\theta_p = 45°$, the amplification makes a diffraction angle θ_{diff} 1.4 times the variation of incident angle θ_{inc}, and the influence from the other-order diffraction light can be prevented. The prism angle of $\theta_p = 45°$ was applied in the following experiments.

2.3 System Analysis

In this study, the PH100-SI-HA-INT-D0 power meter (GENTEC-EO) was used. With a power meter sensor diameter of 10 mm and a laser spot size of 2 mm, based on the optical setup shown in Fig. 1, the CE measurement range is approximately 0.45°, which is sufficient for most optical lens CE measurements.

The lens' CE was determined using the real ray tracing formula [15]. Fig. 7 illustrates the power values obtained within a 30 arc sec range, with the lens vertex as the reference point. With a 5-mW light source, the power meter registered a base power of 2.59 μW. Considering the light source's actual stability, the power meter's resolution was set to 0.005 μW. In the optical setup shown in Fig. 1, the CE resolution achieved was 0.459 arc sec. In comparison, using the same optical setup without SWG, but with a charge-coupled device having a pixel size of 2.2 μm, the CE resolution of an optical system was approximately 2 arc sec. The proposed measurement system in this study achieved a CE resolution four times smaller than typical autocollimation methods.

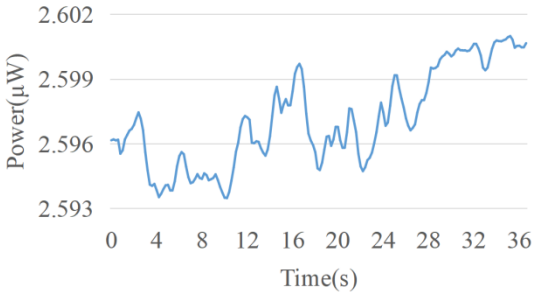

Fig. 7 Measurement result of vertex of lens in 30 s

To ensure measurement stability and account for potential vibration during the rotation process, eight stable lens positions were selected for data acquisition. Fig. 8 illustrates the measurement process using the power meter. As the lens rotates, the reflected light forms an elliptical trajectory on the power meter's receiving surface due to SWG's effect on the diffraction angle. The CE of the central position and its corresponding point can be obtained by averaging the measured power and its variation (ΔP) during rotation, as SWG only affects the power of the light source in the Z direction. The vibration produced by rotation and the edge defect of the lens causes significant pulsation in the power measurement process, as shown in Fig. 9. The average value of each point is measured to obtain stable measurement results. A lens with a curvature radius of 80.261 mm and optical axis error of 19.04 arc sec, as measured using an OptiCentric 100, was tested. The power of the corresponding point and the measured CE are shown in Table 2 and Fig. 9.

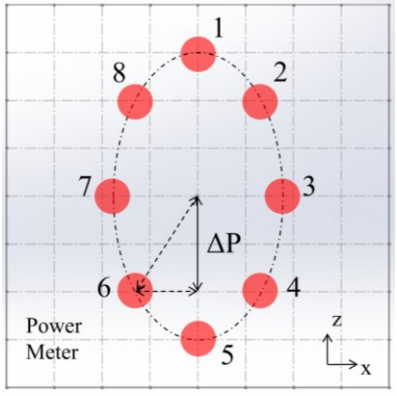

Fig. 8 Laser spot displacement at receiving surface of power meter

Table 2 System measurement result

Position	1	2	3	4	5	6	7	8
Power (μW)	2.625	2.645	2.635	2.650	2.660	2.670	2.575	2.665
CE (arc sec)	14.34	4.02	5.16	8.61	17.79	26.97	60.24	22.38

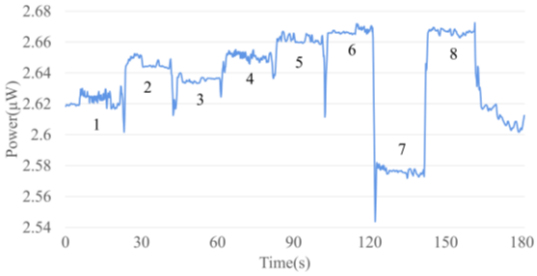

Fig. 10 Power measurement results at eight points.

Based on the measurement results of the aforementioned lens, the range and trend of the power variation were consistent, as expected. In this study, lenses were randomly selected from the factory production line for further measurement. According to the experimental results, under different lens radiuses and different CEs, the errors between the results in this study and those using the OptiCentric 100 were within 1 arc sec.

3. Conclusions

To conclude, this paper introduces a highly accurate technique for measuring the CE of a lens. The method involves power analysis and utilizes a prism with a light pattern generated by a 375-nm SWG combined with a reflection-centering system using -1st-order beams with a 5-mW, 650-nm wavelength laser. The optical power analysis-based CE measurement is affected by ambient light, light source power, and sample reflectance. It proves to be suitable for stable measurement of spherical lenses with reflectance greater than 4%. Notably, the CE resolution achieved in this system is four times higher compared to the conventional autocollimation-based method. The real-world tests conducted on the factory production line demonstrate the feasibility of using SWG for CE measurement, achieving arc sec-level accuracy. The modular design of the optical setup allows for easy replacement of a higher power light source to achieve more stable measurements on coated and low-reflectance surfaces. The key component of the design is the SWG-pasted prism, which effectively amplifies the rate of light direction change and energy variation within the system. This technique can be conveniently implemented by retrofitting existing instruments, making it practical and accessible for various applications.

ACKNOWLEDGEMENT

The authors are grateful for the support of the Research Project of the Ministry of Science and Technology, Taiwan (MOST 110-2222-E-007-009-MY3 and NSTC 111-2622-E-007- 002)

REFERENCES

1.A. L. INGALLS, “Centering of Optical Systems,” JOURNAL OF THE OPTICAL SOCIETY OF AMERICA. VOLUME 38, NUMBER 4 (1948).

2.V. M. Mudholkar and G. K. Sharma, “On centering of lenses during cementing,” Rev. Sci. Instrum. 54, 507–508 (1983).

3.Robert E. Parks, “Lens centering using the Point Source Microscope,” Proc. of SPIE Vol. 6676, 667603 (2007).

4.R. Caputo, L. De Sio, M. J. J. Jak, E. J. Hornix, D. K. G. de Boer, and H. J. Cornelissen, “Short period holographic structures for backlight display applications,” Opt. Express 15(17), 10540–10552 (2007).

5.Chun-Wei Liu, Chun-Che Wu, and Shih-Chieh Lin, “A simple and wide-range refractive index measuring approach by using a sub-micron grating” Appl. Phys. Lett. 106, 151907 (2015).

6. Weifeng Jiang, Jinye Miao, Tao Li, and Lianhao Ma, “On-chip silicon dual-mode multiplexer via a subwavelength grating-based directional coupler and a mode blocker,” Applied Optics Vol. 58, Issue 33, pp. 9290-9296 (2019).

7. Ke Chen, Rui Wu, Hongmei Zheng, Haishuo Wang, Guojun Zhang, and Shunhua Chen, “Light-trapping schemes for silicon thin-film solar cells via super-quadratic subwavelength gratings,” Applied Optics Vol. 58, Issue 31, pp. 8702-8712 (2019).

8. Taban Qayoom and Hakim Najeeb-ud-din, “Comprehensive field pattern analysis for tailoring of reflectance in a hybrid subwavelength plasmonic grating refractive index sensor and its potential for noninvasive salivary glucose monitoring,” Applied Optics Vol. 61, Issue 32, pp. 9429-9438 (2022).

9. Xiaogang Shi, Hong Shen, Zhenghui Xue, and Bingjie Wang, “Subwavelength dielectric grating structures with tunable higher order resonance for achromatic augmented reality display,” Applied Optics Vol. 61, Issue 24, pp. 7245-7254 (2022).

10. Jingjing Guo, Yan Tu, Lanlan Yang, Lili Wang, and Baoping Wang, “Holographic waveguide display with a combined-grating in-coupler”, Applied Optics Vol. 55, Issue 32, pp. 9293-9298 (2016).

11.C. W. Liu, J. Y. and S. C. Lin, "Diamond turning of high-precision roll-to-roll imprinting molds for fabricating subwavelength gratings", Optical Engineering, 55(6) (2016).

12.C. W. Liu, C. H. Lee and S. C. Lin, “Roll-to-roll UV embossing process applied for light bar-based sub-wavelength gratings for backlight”. Journal of the SID 20/12 (2012).

13.S. O. Kasap, Optoelectronics and Photonics: Principles and Practices (Pearson Education Inc., New Delhi, 2009).

14.C. W. Liu, C. H. Lee and S. C. Lin, “Sub-wavelength gratings fabricated on a light bar by roll-to-roll UV embossing process”. Opt. Express 19(12), pp. 11299-11311 (2011).

15.José Sasián, “Introduction to Lens Design,” Chapter 5 - Ray Tracing pp 44-53 (2019)